ON TWINNING-MEDIATED VOID GROWTH IN HEXAGONAL CRYSTALS

Padmeya P. Indurkar,^{1,2} Shailendra P. Joshi,² & A. Amine Benzerga^{3,4,5,*}

Original Manuscript Submitted: 3/9/2022; Final Draft Received: 8/4/2022

Aspects of plastic anisotropy in damage accumulation are considered for a class of hexagonal crystals that deform by combined slip and twinning. Focus is placed on crystallographic aspects that are currently absent from constitutive formulations of ductile damage. To this end, three-dimensional finite-element calculations are carried out using a cubic unit cell containing a single void embedded in a crystal matrix. Plastic flow in the latter is described using crystal plasticity with parameters representative of single crystal pure magnesium. The effect of void oblateness is analyzed in some detail, as voids often form as blunted microcracks in Mg alloys. The analyses reveal two aspects peculiar to twinning-mediated void growth: (1) insensitivity of the effective stress—strain response to void oblateless and (2) a plastic auxetic effect. Both aspects manifest under certain circumstances. Some implications in terms of incorporating the uncovered crystallographic aspects in coupled plasticity-damage formulations of anisotropic materials are discussed.

KEY WORDS: *HCP materials, plasticity, finite elements, void coalescence*

1. INTRODUCTION

Significant progress has been made in recent decades in modeling ductile failure by void nucleation, growth, and coalescence (see, e.g., Benzerga et al., 2016; Noell et al., 2022; Pineau et al., 2016). In particular, various aspects of plastic anisotropy have been incorporated, often from first principles, in porous material plasticity models. This includes incorporating void shape effects (Danas and Ponte Castañeda, 2009; Gologanu et al., 1993, 1997; Madou and Leblond, 2012a,b; Ponte Castañeda and Zaidman, 1994), matrix flow anisotropy (Benzerga and Besson, 2001; Keralavarma and Benzerga, 2008, 2010; Monchiet et al., 2008; Morin et al., 2015; Stewart and Cazacu, 2011), and void coalescence (Benzerga, 2002; Benzerga and Leblond, 2014; Keralavarma and Chockalingam, 2016; Torki et al., 2015). This line of work does not take crystallographic aspects of void growth and coalescence into account. To address these, various constitutive models of porous material crystal plasticity have been proposed in recent years for high-symmetry materials (e.g., Han et al., 2013; Mbiakop et al., 2015; Paux et al., 2015; Song and Ponte Castañeda, 2017). However, the predictive capabilities of porous material crystal plasticity models for hexagonal close packed (HCP) metals have not yet been assessed.†

¹Department of Mechanical Engineering, National University of Singapore, Singapore 117576

²Department of Mechanical Engineering, University of Houston, Houston, TX 77204-4006

³Department of Materials Science and Engineering, Texas A & M University, College Station, TX 77843

⁴Center for Intelligent Multifunctional Materials and Structures, TEES, College Station, TX 77843

⁵Department of Aerospace Engineering, Texas A & M University, College Station, TX 77843

^{*}Address all correspondence to: A. Amine Benzerga, Department of Aerospace Engineering, Texas A & M University, College Station, TX 77843, E-mail: benzerga@tamu.edu

[†]Only recently has such assessment begun (Yang and Ghosh, 2022). At the time of writing, we were not aware of this publication.

To gain insight into the complex interaction between voids, which generally mediate ductile failure, and crystal deformation mechanisms, the voided cell model may be used following earlier paradigms for Mises-like materials (e.g., Koplik and Needleman, 1988; Tvergaard, 1982). Building on earlier work for Hill materials (e.g., Keralavarma et al., 2011), and FCC single crystals (Potirniche et al., 2006; Srivastava and Needleman, 2013; Yerra et al., 2010), various authors have carried out two-dimensional (Prasad et al., 2016) and three-dimensional cell model analyses of void growth in a crystal matrix deforming by combined twinning and slip with the focus generally placed on Mg alloys (Selvarajou et al., 2019) and Ti alloys (Asim et al., 2019). Thus, Selvarajou et al. (2019) considered spherical voids in pure Mg single crystal subjected to various proportional stressing histories and two loading orientations. They found that, beyond mere directionality, the net plastic anisotropy affects the effective response as well as dilatation rates, consistent with homogenization-based models of ductile damage (e.g., Benzerga and Besson, 2001; Keralavarma and Benzerga, 2010). They also observed quite a few crystallographic aspects. Chief among these are mechanisms associated with extension twinning. For example, under c-axis loading, twinning induced crystal reorientation leads to a decrease in void growth rates and eventually to sector formation and quasi-polyhedral void shapes. Such findings elude current constitutive formulations of anisotropic ductile damage.

Quite recently, Indurkar et al. (2022) have analyzed the combined effects of void shape and crystal anisotropy on the effective behavior of unit cells as in Selvarajou et al. (2019). They focused on oblate void shapes, which represent more faithfully the state of incipient damage, say as twin-induced microcracks or nascent voids after particle cracking (Kondori and Benzerga, 2014; Rodriguez et al., 2016). Some findings were common to both spherical and oblate voids. However, with oblate voids failure was found to ensue even under uniaxial loading for both prismatic and c-axis loading. With increasing stress state triaxiality, void oblateness favors extension twinning (which would not be active in the absence of a void) for the prismatic orientation but decreases extension twinning activity for the $\langle c \rangle$ -axis orientation. In addition, when sector formation was favored (i.e., under c-axis loading), the distribution of twin variants around the void was found to be more sensitive to void aspect ratio than to stress triaxiality. The flatter the void, the higher the misorientation across twin sector boundaries, and this presumably plays a key role in premature failure.

One issue with the analyses in Indurkar et al. (2022) is the extent to which the obtained trends are sensitive to the idealized representation. For example, a single-void analysis does not take into account intrinsic void interactions, which would require analyses with multiple voids. Likewise, the growth of the voids in polycrystals may be affected by grain boundaries or texture effects depending on void size relative to the grain size (Azghandi et al., 2020). At present, investigating such aspects would require large computational resources. Also, the analyses in Indurkar et al. (2022) were carried out at a fixed initial void volume fraction. This implies that when void oblateness effects were investigated (by varying the initial void aspect ratio) the relative ligament size was also varied. The extent to which such variations affect damage progression to failure can only be ascertained if a complementary set of calculations fixing the relative ligament parameter are conducted. This is precisely the aim of this paper. In doing so, special attention is paid to early stages of void growth, which reveal an auxetic effect. Implications of such fine details in ductile damage remain to be fully investigated. Throughout the paper, second- and fourth-order tensors are denoted by bold and double-stroke symbols, respectively, e.g., I and I; the contracted product, inner product, and dyadic product are such that $\mathbb{A}: \mathbf{B} = A_{ijkl}B_{kl}$, $\mathbf{AB} = A_{ik}B_{kj}$, and $\mathbf{A} \otimes \mathbf{B} = A_{ij}B_{kl}$ in component form. Similarly, given vectors a and b, one has $\mathbf{a} \otimes \mathbf{b} = a_ib_i$ and $\mathbf{a} \cdot \mathbf{b} = a_ib_i$.

2. FORMULATION

An oblate void of aspect ratio W_0 is placed at the center of a cubic unit cell, Fig. 1. When the cell is subjected to transversely isotropic loading (with respect to the void axis) it deforms into a rectangular prism with current dimensions L_x , L_y , and L_z ; see Fig. 1(b). The initial cell aspect ratio is denoted by $\lambda_0 = L_{y0}/L_{x0} = L_{y0}/L_{z0}$ with 0 referring to the initial state. Here, $\lambda_0 = 1$. Since the crystalline matrix is anisotropic, the void deforms into a three-dimensional shape with principal radii r_x , r_y , and r_z . In the transverse plane (plane of potential coalescence) two ligament parameters may be introduced: $\chi_x = 2r_x/L_x$ and $\chi_z = 2r_z/L_z$ with $\chi_{x0} = \chi_{z0} = \chi_0$, the initial ligament parameter.

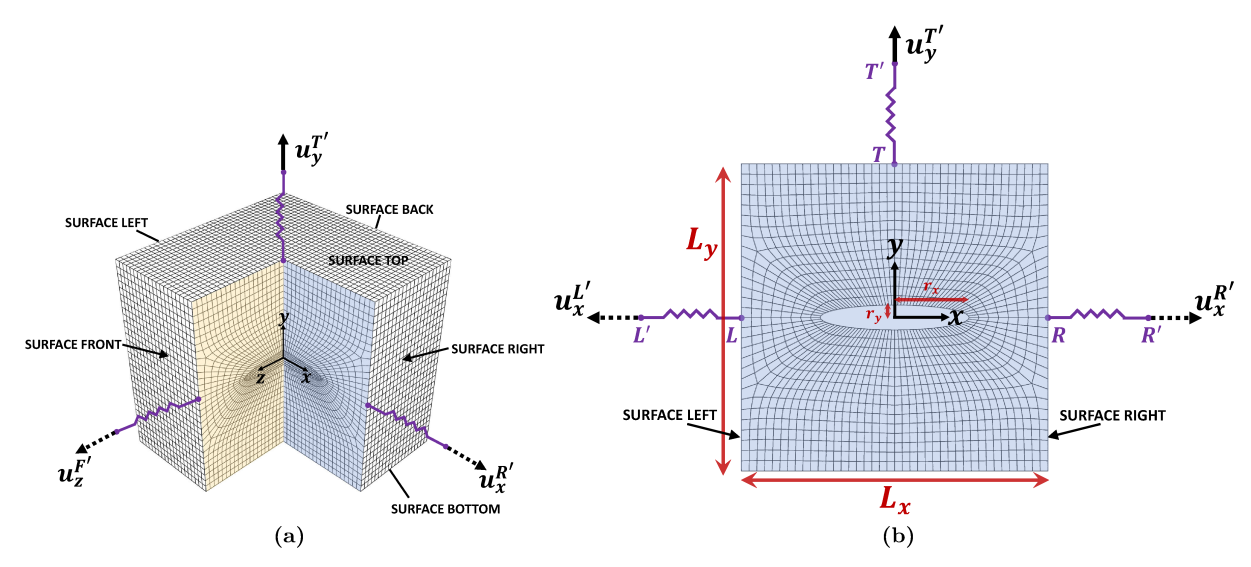


FIG. 1: The unit cell with key dimensions and loading setup: (a) typical finite element mesh (here for $W_0 = 1/6$); and (b) section in central xy-plane

Since only cubic cells are initially considered, the initial void volume fraction f_0 is not independent of W_0 and χ_0 . In a companion paper (Indurkar et al., 2022), the effect of the void aspect ratio W_0 was analyzed at fixed f_0 . Here, analyses are carried out at fixed ligament parameter χ_0 . As will be discussed later, there is interest in considering both situations based on an earlier study by Lassance et al. (2006) in which the matrix was taken to obey J_2 flow theory and subsequent extension to Hill materials by Keralavarma et al. (2011).

Cell-level stress and strain measures are defined as

$$\Sigma_{ij} = \frac{1}{V} \int_{V} \sigma_{ij} \, dV; \qquad E_{xx} = \ln\left(\frac{L_x}{L_{x0}}\right); \quad E_{yy} = \ln\left(\frac{L_y}{L_{y0}}\right); \quad E_{zz} = \ln\left(\frac{L_z}{L_{z0}}\right)$$
(1)

with σ the Cauchy stress and V the unit cell volume. Note that $E_{xx} \neq E_{zz}$. Then define

$$\Sigma_m = \frac{1}{3} \mathbf{\Sigma} : \mathbf{I}; \qquad \Sigma_{eq} = \sqrt{\frac{3}{2} \mathbf{\Sigma}' : \mathbf{\Sigma}'}; \qquad \mathbf{\Sigma}' = \mathbb{J} : \mathbf{\Sigma}; \qquad \mathbf{E}_{eq} = \sqrt{\frac{2}{3} \mathbf{E}' : \mathbf{E}'}$$
 (2)

as the mean normal stress, von Mises equivalent stress, stress deviator, and equivalent strain, respectively. Here, $\mathbb{J} = \mathbb{I} - (1/3) \mathbf{I} \otimes \mathbf{I}$ is the deviatoric projector.

The stress state is characterized using the triaxiality ratio $\mathcal{T} = \Sigma_{\rm m}/\Sigma_{\rm eq}$ with a major axial stress, i.e., $\Sigma_{yy} \ge \Sigma_{xx} = \Sigma_{zz}$.

Calculations are carried out for proportional stressing histories. This implies fixed triaxiality \mathcal{T} ; see Indurkar et al. (2022) and references therein for details.

A constitutive relation of crystal plasticity (Zhang and Joshi, 2012) is used for the matrix material, which accounts for finite deformations, rate dependence, slip, and twinning, as in previous studies (Selvarajou et al., 2019, 2016). The deformation gradient \mathbf{F} is multiplicatively decomposed into an elastic part, \mathbf{F}^e , and a plastic part, \mathbf{F}^p . The plastic part of the the velocity gradient is then

$$\mathbf{L}^p = \mathbf{F}^e \dot{\mathbf{F}}^p \mathbf{F}^{p-1} \mathbf{F}^{e-1} \tag{3}$$

where a dot stands for the material derivative. The flow rule is written as

$$\mathbf{L}^{p} = \underbrace{\left(1 - \sum_{\beta=1}^{N_{\text{tw}}} f^{\beta}\right) \sum_{\alpha=1}^{N_{s}} \dot{\mathbf{\gamma}}^{\alpha} (\mathbf{s}^{\alpha} \otimes \mathbf{m}^{\alpha})}_{\text{slip in parent}} + \underbrace{\sum_{\beta=1}^{N_{\text{tw}}} \dot{\mathbf{\gamma}}^{\beta} (\mathbf{s}^{\beta} \otimes \mathbf{m}^{\beta})}_{\text{twin in parent}}$$
(4)

70 Indurkar, Joshi, & Benzerga

where N_s and $N_{\rm tw}$ are the numbers of slip and twin systems in the parent region, respectively, \mathbf{m}^i and \mathbf{s}^i denote the current slip/twin plane normal and direction vectors, respectively. The notation $i=\alpha$ for slip and $i=\beta$ for twinning is merely for convenience. Also, f^{β} is the twin volume fraction associated with the β th twin system and $\dot{\gamma}^i$ is the shear rate on the *i*th system.

For slip, it is given by:

$$\dot{\gamma}^i = \dot{\gamma}_0 \left| \frac{\tau^i}{g^i} \right|^{1/m} \operatorname{sgn}(\tau^i); \qquad g^i = \tau_0^i + \int_0^t (\dot{g}_{\rm sl}^i + \dot{g}_{\rm tw-sl}^i) \, \mathrm{d}t$$
 (5)

where $\dot{\gamma}_0$ is a reference slip rate, $\tau^i = \mathbf{\sigma} : (\mathbf{m}^i \otimes \mathbf{s}^i)$ is the resolved shear stress (RSS), g^i is the current strength of the slip system, and m is the rate-sensitivity exponent. In Eq. (5)₂, τ^i_0 is the initial critical RSS, t is time, and $\dot{g}^i_{\rm sl}$ represents hardening due to slip given by

$$\dot{g}_{\rm sl}^i = \sum_{i=1}^{N_s} h_{ij} \dot{\gamma}^j \tag{6}$$

where h_{ij} are hardening moduli that depend on the total accumulated shear due to slip, $\bar{\gamma}$, via:

$$h_{ij}(\bar{\gamma}) = \begin{cases} h(\bar{\gamma}) & (i = j, \text{ self hardening}) \\ qh(\bar{\gamma}) & (i \neq j, \text{ latent hardening}) \end{cases}; \qquad \bar{\gamma} = \sum_{i=1}^{N_s} \int_0^t \dot{\gamma}^i$$
 (7)

with q the latent hardening coefficient and

$$h(\bar{\gamma}) = \begin{cases} h_0^i, & \text{(basal slip)} \\ h_0^i \text{sech}^2 \left| \frac{h_0^i \bar{\gamma}}{\tau_s^i - \tau_0^i} \right|, & \text{(nonbasal slip)} \end{cases}$$
 (8)

Here, h_0^i is the initial hardening modulus and τ_s^i is the saturation stress of the *i*th slip system. The preceding hardening equations are motivated by experiments on Mg single crystals.

The last term in Eq. (5)₂ represents the effect of twinning on slip hardening and is given by

$$\dot{g}_{\text{tw-sl}}^{i} = \sum_{\beta=1}^{N_{\text{tw}}} h_{i\beta} \dot{\gamma}^{\beta} \tag{9}$$

Slip hardening is taken to be independent of slip system and saturating when affected by extension twinning (ET) or nonsaturating when affected by contraction twinning (CT) such that:

$$h_{i\beta} = \begin{cases} h_{\text{et-sl}}^{\beta} \operatorname{sech}^{2} \left| \frac{h_{\text{et-sl}}^{\beta} \bar{\gamma}_{\text{et}}}{\tau_{s}^{\beta} - \tau_{0}^{\beta}} \right| & (\text{ET on slip}) \\ \frac{1}{2} H_{\text{ct-sl}} / \sqrt{\bar{\gamma}_{\text{ct}}} & (\text{CT on slip}) \end{cases}$$
(10)

where

$$\bar{\gamma}_{\text{et}} = \sum_{\beta=1}^{N_{\text{et}}} \int_{0}^{t} \dot{\gamma}^{\beta} \quad \text{and} \quad \bar{\gamma}_{\text{ct}} = \sum_{\beta=1}^{N_{\text{ct}}} \int_{0}^{t} \dot{\gamma}^{\beta}$$
(11)

with $N_{\rm et}$ and $N_{\rm ct}$ being the numbers of ET and CT variants, respectively (with $N_{\rm et}+N_{\rm ct}=N_{\rm tw}$). The ET related parameters in Eq. (10)₁ have similar meaning as for nonbasal slip; see Eq. (8). The factor 1/2 is introduced in Eq. (10)₂ such that $H_{\rm ct-sl}$ represents the initial slip hardening rate due to CT.

The last term in the flow rule, Eq. (4), involves the shear rate for the β th twin system:

$$\dot{\gamma}^{\beta} = \dot{f}^{\beta} \gamma^{\text{tw}}; \qquad \dot{f}^{\beta} = \dot{f}_0^{\beta} \left(\frac{\tau^{\beta}}{s^{\beta}}\right)^{1/m_t} \tag{12}$$

where f^{β} , τ^{β} , and s^{β} respectively denote the twin volume fraction, RSS, and current strength, all associated with the β th twin system. Also, γ^{tw} is the theoretical twinning shear. The strength is specified through

$$s^{\beta} = \tau_0^{\beta} + \int_0^t (\dot{s}_{\text{tw}}^{\beta} + \dot{s}_{\text{sl-tw}}^{\beta}) dt$$
 (13)

The contribution of twin-twin interactions is given by

$$\dot{s}_{\text{tw}}^{\beta} = \begin{cases} h_{\text{et}}^{\beta} \text{sech}^{2} \left| \frac{h_{\text{et}}^{\beta} \bar{\gamma}_{\text{et}}}{\tau_{s}^{\beta} - \tau_{0}^{\beta}} \right| \dot{\gamma}^{\beta} & (\text{ET}) \\ H_{\text{ct}} \left(\sum_{m=1}^{N_{\text{ct}}} f_{m} \right)^{b} \dot{\gamma}^{\beta} & (\text{CT}) \end{cases}$$

$$(14)$$

The hardening of ET systems is controlled by parameter $h_{\rm et}^{\beta}$ and that of CT systems by $H_{\rm ct}$ and exponent b. Also, f_m denotes the twin volume fraction for the mth CT variant. Finally, the effect of slip on twin-system hardening is neglected, i.e., $\dot{s}_{\rm sl-tw}^{\beta}=0$, as in Zhang and Joshi (2012).

Twinning-induced lattice reorientation is taken to occur when the accumulated twin volume fraction, $\bar{f} = \sum_{i}^{N_{\text{tw}}} f_i$, reaches a critical value f_{cr} . The twin system that possesses the largest twin volume fraction is chosen as the orientation of the twinned lattice.

3. RESULTS

Material parameters representative of pure Mg single crystals are used; see Indurkar et al. (2022) and references therein. The elastic stiffness tensor is taken to be transversely isotropic with the five independent moduli given by $C_{11} = 59.40$, $C_{12} = 25.61$, $C_{13} = 21.40$, $C_{33} = 61.60$, and $C_{44} = 16.40$ (all in GPa). Table 1 lists all slip and twin systems considered in the crystal plasticity formulation. Thus, $N_s = 18$ and $N_{tw} = 12$.

systems considered in the crystal plasticity formulation. Thus, $N_s=18$ and $N_{\rm tw}=12$.

Also, $\dot{\gamma}_0=0.001~{\rm s}^{-1}$; $m=m_t=0.02$; q=1; $\gamma^{\rm tw}=0.129$ and 0.138 for ET and CT, respectively, $\dot{f}_0^{\,\beta}=0.001s^{-1}$ for all ET systems, and $\dot{f}_0^{\,\beta}=0.0001s^{-1}$ for all CT systems. In addition, the initial and saturation strengths as well as the initial hardening rates for all deformation systems are listed in Table 2 where superscripts for slip and twin systems are dropped. Where applicable, note that the same parameters are used for each ET or CT system; see Eqs. (10) and (14).

Two crystal orientations are considered (see Table 3), as in Selvarajou et al. (2019) and Indurkar et al. (2022). For the $[1\bar{2}10]$ orientation, prismatic slip is expected to be dominant under uniaxial loading without a void. Also, large anisotropy is expected in the transverse ($[1\bar{2}10] - [0001]$) plane. On the other hand, for the [0001] orientation, extension twinning is favored under uniaxial loading without a void and transverse anisotropy is not expected to be strong before reorientation.

In all calculations, the initial ligament parameter $\chi_0 = 0.2673$ and the initial cell aspect ratio $\lambda_0 = 1$ are kept fixed; see Fig. 1. Three values of the initial void aspect ratio are considered; see Table 4. The corresponding values

	Slip/twin plane	Slip/twin direction	Number of systems		
Basal $\langle a \rangle$ slip	(0001)	$\langle 11\bar{2}0\rangle$	3		
Prismatic $\langle a \rangle$ slip	$\{10\bar{1}0\}$	$\langle 11\bar{2}0 \rangle$	3		
Pyramidal $\langle a \rangle$ slip	$\{10\bar{1}1\}$	$\langle 11\bar{2}0 \rangle$	6		
Pyramidal $\langle c+a \rangle$ slip	$\{11\bar{2}2\}$	$\langle 11\bar{2}3 \rangle$	6		
Extension twinning	$\{10\bar{1}2\}$	$\langle 10\bar{1}1 \rangle$	6		
Contraction twinning	$\{10\bar{1}1\}$	$\langle 10\bar{1}\bar{2}\rangle$	6		

TABLE 1: Slip and twin systems in pure Mg

72 Indurkar, Joshi, & Benzerga

	τ ₀ (MPa)	h ₀ (MPa)	τ_s (MPa)	
Basal slip	0.5	20	_	
Prismatic $\langle a \rangle$ slip	25	1500	85	
Pyramidal $\langle a \rangle$ slip	25	1500	85	
Pyramidal $\langle c+a \rangle$ slip	40	3000	150	
	τ ₀ (MPa)	h _{et} (MPa)	τ_s (MPa)	$h_{\mathrm{et-sl}}$ (MPa)
Extension twinning	3.5	100	20	100
	τ ₀ (MPa)	H _{ct} (MPa)	$H_{\mathrm{ct-sl}}$ (MPa)	b
Contraction twinning	55	6000	15	0.05

TABLE 2: Strength and hardening parameters used for pure Mg

TABLE 3: Crystal and global (in parenthesis) orientations considered in this work

Orientation	Loading direction (y)	Lateral direction (x)	Lateral direction (z)
Prismatic	$[1\bar{2}10]$	$[10\overline{1}0]$	[0001]
$\langle c \rangle$ -axis	[0001]	$[1\bar{2}10]$	$[10\overline{1}0]$

TABLE 4: Initial porosity configurations in a cubic cell ($\lambda_0 = 1$) at fixed ligament parameter

W_0	χ ₀	f_0
1/10	0.2673	0.001
1/20	0.2673	0.0005
1/30	0.2673	0.00033

of the initial void volume fraction f_0 are also listed. This is in addition to the reference case of a spherical void $(W_0 = 1)$ taken from Selvarajou et al. (2019). As noted after Eq. (2), the loading is triaxial with equilateral stresses $(\Sigma_{xx} = \Sigma_{zz})$ and the range of triaxiality considered is $\mathcal{T} = 1/3$ to $\mathcal{T} = 3$. Several values of \mathcal{T} within this range were explored; however, the results herein focus on end values for brevity.

The unit cell is discretized using $\sim 60,000$ fully integrated linear hexahedral (C3D8) elements in ABAQUS/STANDARD. When possible, calculations are pursued until after the onset of void coalescence, i.e., when the cell's mode of deformation shifts to uniaxial stretching (Koplik and Needleman, 1988). This is simply detected by the saturation of the overall lateral strains (E_{xx} and E_{zz}). In some cases, such transition does not occur.

First, consider the T = 1/3 case (uniaxial tension). Figure 2 shows macroscopic responses along with the corresponding evolution of void volume fraction for various values of the initial void aspect ratio. The response of the void-free (pristine) matrix is shown for reference.

For prismatic loading (right plots), the stress–strain response of the pristine material is dominated by prismatic slip with early saturation hardening at $\Sigma_{\rm eq} \sim 200$ MPa [see Fig. 2(a)]. Considering the porosity level ($f_0 = 0.01$ or below), the response of the voided cell is always weaker than the matrix. The key observation, however, is that the $W_0 = 1/10$, $W_0 = 1/20$, and $W_0 = 1/30$ responses corresponding to penny-shaped cracks are indistinguishable from each other and even close to the $W_0 = 1$ case (solid red curve; color online). On the other hand, the evolution of void volume fraction does depend on W_0 , as shown in Fig. 2(b) (right plot). The rate of increase is higher for the most oblate void. This is in spite of a decreasing level of initial porosity with increasing oblateness; recall that the calculations are run at a constant χ_0 . Also note that the porosity curves are concave downward.

For c-axis loading, the trends are essentially the same in terms of insensitivity of the effective stress to the magnitude of oblateness despite the corresponding effect on porosity evolution (see left plots in Fig. 2). Here, two

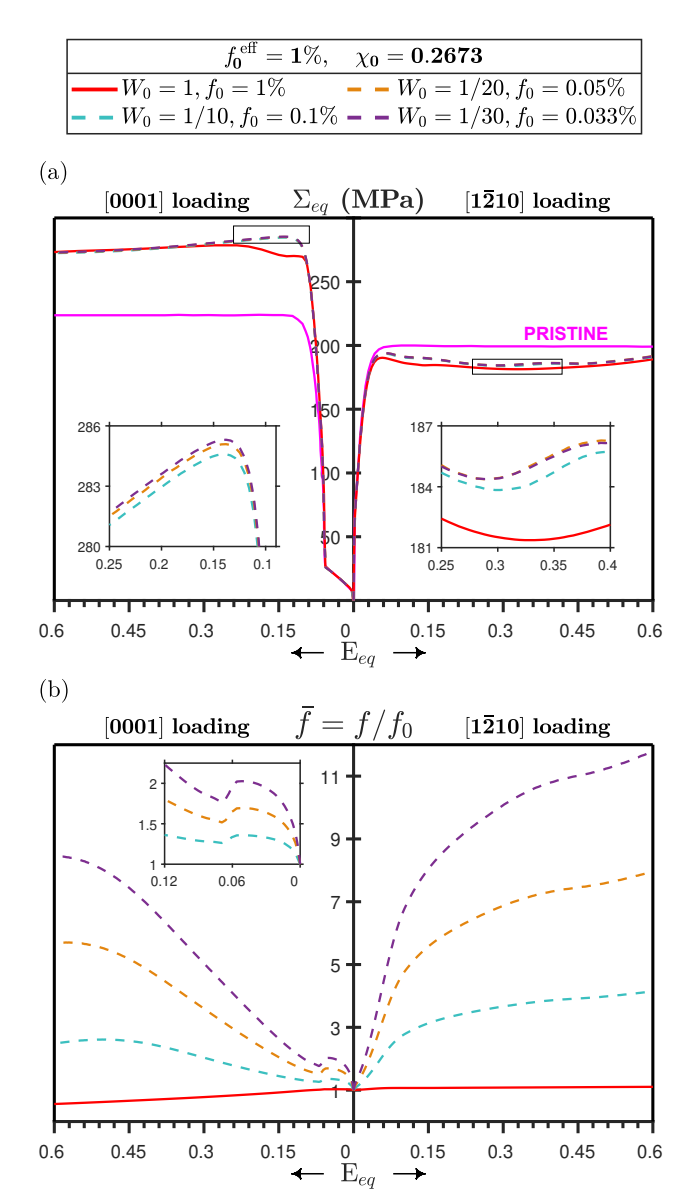


FIG. 2: Orientation dependent (a) effective stress $\Sigma_{\rm eq}$ and (b) normalized porosity f/f_0 versus effective strain $E_{\rm eq}$ for various values of the void aspect ratio W_0 , $\chi_0=0.2673$, and $\mathcal{T}=1/3$

observations are worth making. First, the voided cell is harder than the pristine matrix for all cases considered. This arises due to the formation of twin sectors that activate harder systems of nonbasal slip. Initial yield in the void-free matrix occurs due to ET, followed by rapid hardening due to activity on nonbasal systems resulting from twinning-induced crystal reorientation until saturation eventually ensues [see Fig. 2(a) (left)]. Second, there is a net porosity decrease in the $W_0=1$ case, which is due to lateral shrinking of the void that remains uncompensated for by the lateral shrinking of the cell (Selvarajou et al., 2019). A similar trend is seen here for the $W_0=1/10$ case at larger strains.

The results in Fig. 2 stand in contrast to those of Indurkar et al. (2022) who varied the initial ligament parameter χ_0 while keeping the initial void volume fraction f_0 constant. They found that the flatter the void the weaker the cell and that subsequent hardening of the cell depended on microstructure evolution.

Under uniaxial loading, failure by the onset of coalescence did not occur for either loading orientation. On this too, some results are in contrast with those of Indurkar et al. (2022) where failure under uniaxial loading was noted in some cases due to higher porosity levels.

Next, consider the case of highly triaxial loading with $\mathcal{T}=3$, Fig. 3. Now, the voided cell is significantly weaker than the matrix, irrespective of (main) loading orientation. An exception is noted in the linear hardening regime after twinning is complete under c-axis loading [see Fig. 3(a) (left)]. Here too, the $W_0=1/10$, $W_0=1/10$, and $W_0=1/10$ 0 responses are indistinguishable from each other [Fig. 3(a)] in spite of differing porosity levels [Fig. 3(b)]. However, under high triaxiality the responses of the cells containing penny-shaped cracks differ quite substantially from the response of the cell with a spherical void (solid red lines; color online). For prismatic loading, such differences are noted from the outset of plastic flow. On the other hand, for c-axis loading differences only emerge after

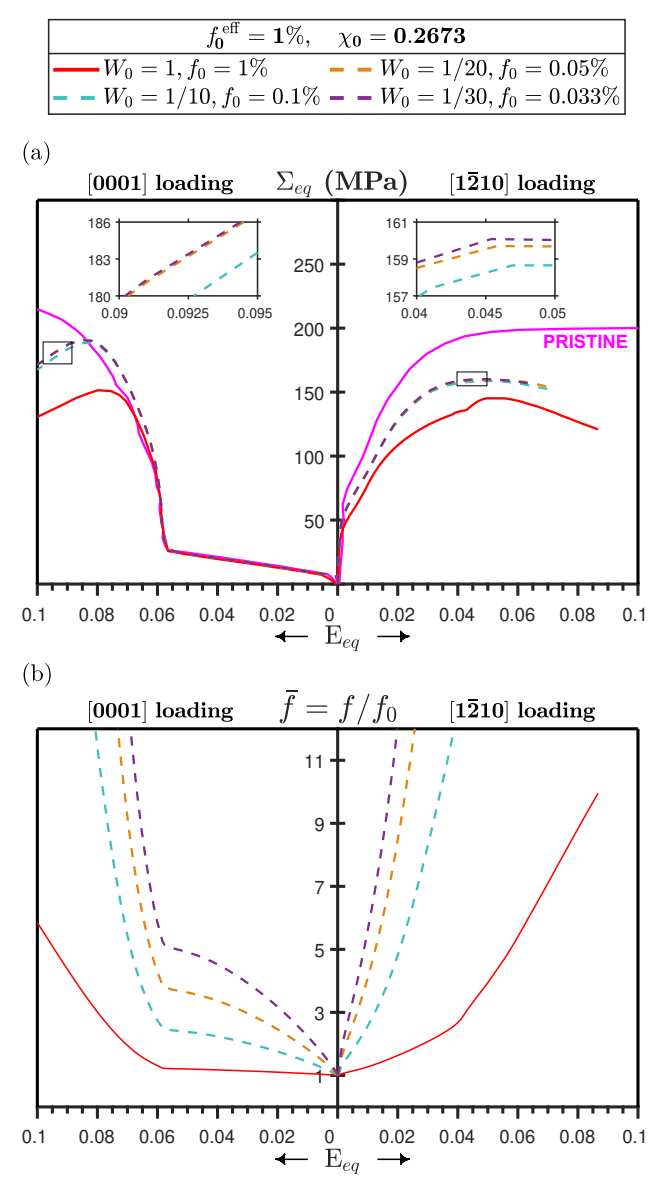


FIG. 3: Orientation dependent (a) effective stress $\Sigma_{\rm eq}$ and (b) normalized porosity f/f_0 versus effective strain $E_{\rm eq}$ for various values of the void aspect ratio W_0 , $\chi_0=0.2673$, and $\mathcal{T}=3$

twinning is complete. All of this merits further discussion later. At high triaxiality, failure by void coalescence is obtained, as expected. However, this aspect is not emphasized here.

Figure 3(b) shows the evolution of normalized porosity versus equivalent strain for all cases considered. Overall, the curves are concave upward, unlike the uniaxial loading case [compare with Fig. 2(b)]. An exception is noted during the twinning dominated regime for c-axis loading. Here, the results are given in terms of normalized porosity because the initial values are vastly different as per the constant χ_0 prescription. On the other hand, the reader should be warned that the aboslute porosity is much larger in the $W_0 = 1$ case than in other cells.

Under prismatic loading, an auxetic behavior was noted. Recall that plastic deformation in this case is highly anisotropic. This has an interesting effect on the nature of unit cell deformation as reported in Fig. 4. For a plastically isotropic material, the cell laterally shrinks as it extends axially. This reflects in negative values of lateral strains E_{zz} and E_{xx} , as represented using dashed lines in Fig. 4. The same behavior is generally observed in conventional anisotropic materials (Keralavarma et al., 2011). As shown in Fig. 4, a transient auxetic behavior is observed for all triaxiality levels considered. The effect is observed in the z-direction, which corresponds to the c-axis (see Table 3). Lateral strain E_{xx} is always negative (not shown here).

The auxetic effect results from a combination of factors. First, in the pristine matrix it is difficult to contract the *c*-axis. This is estimated in Fig. 4 based on how far the corresponding curves (shown pink) are from the isotropic reference case (dashed). Second, this trend is exacerbated in the presence of a void. The flatter the void, the stronger the effect. In all cases, the effect is transient in that a decrease in lateral strain is eventually observed after sufficient straining.

Further, this auxetic behavior depends on stress triaxiality. For low levels of triaxiality ($\mathcal{T} \lesssim 1$) and less oblate voids ($W_0 \gtrsim 1/6$), $E_{zz} \approx 0$. At higher levels of triaxiality ($\mathcal{T} \sim 1$) and for more oblate voids, $E_{zz} > 0$ over a certain range of deformation before transitioning to $E_{zz} < 0$. At very high triaxiality levels ($\mathcal{T} \sim 3$), E_{zz} is always positive. In essence, the cell has the tendency to behave in a plastically auxetic manner along the direction that is plastically harder. As discussed by Selvarajou et al. (2019) in the context of spherical voids, this behavior is a direct result of extension twinning. However, in that work this type of behavior was observed only at very high levels of triaxiality. On that background, the present results highlight the role of void oblateness: the more oblate the void, the higher the tendency of the cell to behave in a directionally auxetic manner. Moreover, the oblateness can drive such a behavior even at modest levels of triaxiality.

4. DISCUSSION

Previous analyses of void growth and coalescence in hexagonal crystals have highlighted the important role of crystal plasticity mechanisms, for example in twin sector formation (Selvarajou et al., 2019) and its extreme sensitivity to void shape (Indurkar et al., 2022). Here, further insight is obtained by presenting complementary analyses. By way of comparison, the calculations of Indurkar et al. (2022) were carried out at fixed initial porosity $f_0 = 0.01$. This

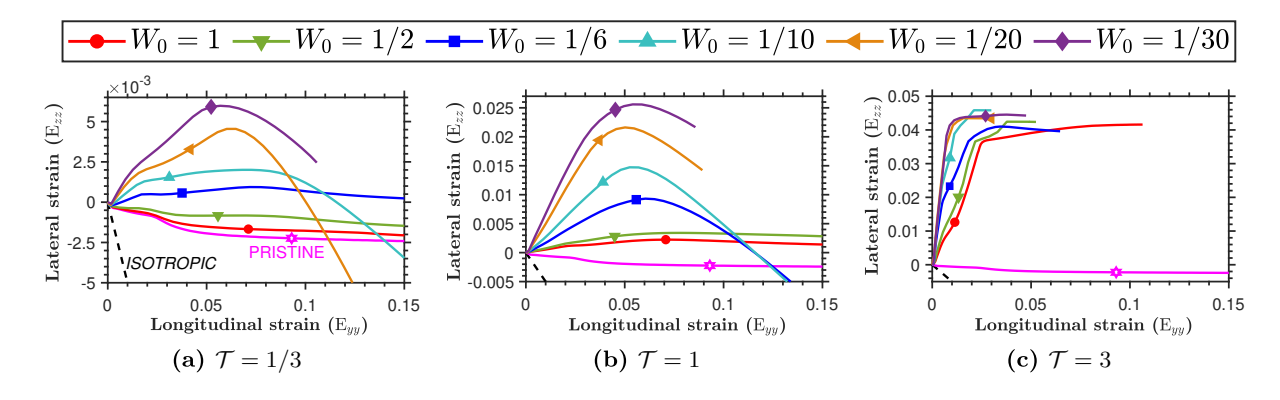


FIG. 4: Evolution of lateral strain E_{zz} under prismatic loading for different stress triaxialities

amounted to varying the initial ligament parameter in the range $0.27 \le \chi_0 \le 0.83$. Here, a single ligament parameter is considered (see Table 4). Consequently, the results are quite different from those of Indurkar et al. (2022). The effective stress (flow stress of the porous material) is found to be insensitive to how oblate the void is, and this holds for both loading orientations at all stress triaxiality levels considered; see Figs. 2(a) and 3(a).

One possible interpretation of the insensitivity to W_0 of the effective stress is that the latter is governed by the initial ligament parameter χ_0 . The results of Indurkar et al. (2022) who varied χ_0 at constant f_0 give credence to this interpretation. However, this may be an appearance only. Indeed, note the modest levels of void volume fraction reached in the present calculations. For example, for $\mathcal{T}=1/3$ in spite of an order of magnitude increase in porosity [Fig. 2(b)], the porosity maxima are still below 0.01 when the calculations are stopped (at $E_{\rm eq} \sim 0.6$). For reference, 0.01 is the value of f_0 for the $W_0=1$ case. By way of contrast, the porosity was always higher than 0.01 in the calculations of Indurkar et al. (2022) although the ratios f/f_0 vary within an order of magnitude in all cases considered here and in Indurkar et al. (2022). So there seems to be a cutoff value of porosity (around 0.01) below which the stress-strain response of the voided cell is mostly controlled by χ_0 , in which case the values of either f_0 or W_0 play a negligible role.

The role of penny-shaped cracks in idealizing incipient states of void nucleation is important in a variety of material systems. Because of this a limited number of studies had previously addressed the combined effects of initial void volume fraction and initial ligament parameter by means of the voided cell model. Thus, Lassance et al. (2006) carried out such analyses for an isotropic matrix. Later, Keralavarma et al. (2011) analyzed in further detail the role of plastic anisotropy in the context of Hill materials.

For isotropic materials with highly oblate voids, Lassance et al. (2006) observed that the stress-strain responses were insensitive to W_0 (for a given χ_0) and attributed that to *porosity equivalence*. They introduced an effective initial porosity defined as the ratio of the actual void volume fraction and the void aspect ratio: $f_0^{\text{eff}} = f_0/W_0$. For a cubic cell $\lambda_0 = 1$ such that the ligament parameter can be written as

$$\chi_0 = \left(\frac{1}{\gamma} \frac{f_0}{W_0}\right)^{1/3} \tag{15}$$

where γ is a constant factor that represents the shape of the cell ($\pi/6$ for the cubic cell). Hence, $f_0^{\rm eff} = \gamma \chi_0^3$ so that keeping χ_0 constant when exploring the effect of void oblateness amounts to keeping the initial value of effective porosity constant. In all calculations reported here we have $f_0^{\rm eff} = 0.01$.

Clearly, the results in terms of effective stress and for $\mathcal{T}=1/3$ support this effective porosity concept. Not only is the stress-strain curve independent of how oblate the void is, the three curves for oblate voids are quite close to that of a spherical void, for which $f_0=0.01=f_0^{\rm eff}$. However, unlike the results of Lassance et al. (2006) the evolution of void volume fraction is highly dependent upon W_0 . An even more significant departure from the effective porosity paradigm is noted at high triaxiality. For $\mathcal{T}=3$, the effective stress responses under $\langle c \rangle$ -axis loading are insensitive to W_0 in the twinning regime ($E_{\rm eq} \lesssim 0.06$) but are sensitive to W_0 after twinning. According to Lassance et al. (2006), porosity equivalence is a consequence of the competing effects of increasing W_0 , which promotes softening, and decreasing f_0 (for a fixed $f_0^{\rm eff}$), which retards it. Keralavarma et al. (2011) showed that Hill-anisotropic materials that are weak in shear exhibit stress-strain responses are insensitive to W_0 whereas shear resistant materials are sensitive to W_0 . In other words, only shear-weak materials comply with the notion of porosity equivalence. Against that backdrop, the insensitivity to W_0 during the twinning regime is a result of the shear-weak orientation. After twinning is complete, however, the crystal exhibits a shear resistant response (due to the activation of nonbasal slip) that is sensitive to W_0 . Under prismatic axis loading (at $\mathcal{T}=3$), the material exhibits a shear-resistant response that is sensitive to W_0 , which is analogous to the post-twinning response under $\langle c \rangle$ -axis loading. Therefore, in general, porous HCP crystals do not espouse the notion of porosity equivalence.

The fact that penny-shaped voids, such as those considered here, are representative of voids initiated as second-phase particles is less questionable than for twin-induced microcracks. It is often reported that twin tips are severe stress concentration points due to pile-up of zonal dislocations and can trigger brittle fracture in the adjacent matrix. For this reason, twin-induced microcracks would extend following a Griffith–Orowan process and not by a growth and coalescence process, as would be the case for microvoids triggered by particle cracking. Should that scenario be

the dominant one indeed, the present simulations would not apply until some brittle fracture criterion is incorporated in the matrix. A few points are worth mentioning, however. First, Rodriguez et al. (2016) have reported extensive blunting and growth of twin-induced microcracks (at sufficient temperature). Also, Kondori and Benzerga (2014) have shown evidence of dimpled fracture in moderately notched bars whereas the quasi-cleavage aspects were only reported in severely notched bars. Whether a Griffith theory can rationalize such facts remains to be explored. On the other hand, Kondori and Benzerga (2017) have shown that a model based on void growth and coalescence can account for all facts, and in particular predict quasi-brittle, triaxiality-dependent fracture, provided void shape effects are taken into consideration.

The plastic auxetic effect under prismatic slip may have practical implications in failure that have not thus far received the attention they deserve. The difficulty in contracting the c-axis is evident from how far the corresponding lateral strain is from the isotropic reference [see curve labeled "pristine" in Fig. 4(a)]. This trend has been reported experimentally, e.g., by Kondori and Benzerga (2014) in polycrystalline Mg alloy with a basal texture [see their Fig. 4(b)]. All proportions kept, one common consequence in both the experiments and unit cell simulations is that the other lateral direction *a fortiori* accumulates more plastic strain. In the simulations, plastic incompressibility of the matrix is imposed so that straining along $\begin{bmatrix} 10\overline{1}0 \end{bmatrix}$ is maximized so as to compensate for the lack of deformability along the c-axis. Interestingly, Kondori and Benzerga (2014) reported smaller lateral strains than simulated here, and this implied plastic dilatation. In the presence of a void in the simulations, the material is overall plastically compressible. Therefore, void growth mediates apparently positive lateral strains along the c-axis. Indeed, the matrix itself does not deform or deforms very little, but the void boundaries move outward along the c-axis. This explains the trends seen for example in Fig. 4. Accordingly, the higher the rate of void growth, the larger the auxetic effect. This explains the effect of stress triaxiality seen in Fig. 4. In practice, the effect may be local, and because of the potential strain incompatibility that results from confining grains or the like, failure may ensue locally. There is very little documentation of such effects in currently available experimental reports.

The material parameters used in the analyses carried out here are representative of single crystal pure Mg. Although some generic aspects of orientation and crystallographic effects remain relevant for both Mg alloys and other HCP metals, care should be taken in generalizing all findings to other material systems. Some observations along these lines were made by Selvarajou et al. (2017) in the context of textural effects in Mg alloys. More work is needed in this area to uncover other aspects of void growth and coalescence in HCP metals.

5. CONCLUSION

The growth of initially oblate voids representing incipient damage in a class of HCP single crystals has been examined under tensile loading in some detail. Complementary to a companion study, focus has been placed on keeping the initial ligament size (relative to void spacing) constant when varying the void aspect ratio. From the analyses two aspects of twinning-mediated void growth emerge:

- The insensitivity of the effective response to void oblateness noted in isotropic materials has been shown to be limited to situations where twinning is active and the void volume fraction is low. When twinning is inactive or complete (depending on the initial loading orientation) a significant effect of the void aspect ratio is observed on the stress–strain curve. Also, in all cases, the evolution of void volume fraction is sensitive to void oblateness, unlike in plastically isotropic materials.
- In addition, a plastic auxetic effect is observed under situations where the c-axis is induced to contract, such as under prismatic loading here. Under more realistic conditions of plastic confinement by neighboring grains, such local effects may lead to microcrack initiation and premature failure. Such aspects would merit examination based on careful experiments.

ACKNOWLEDGMENTS

SPJ and AAB acknowledge support provided by the National Science Foundation under "Collaborative Research: Multiscale Modeling of Damage Tolerance in Hexagonal Materials" (Grant Nos. CMMI-1932976 to SPJ and

CMMI-1932975 to AAB). PPI acknowledges support from NUS Research Scholarship and funding support from the Army Research Laboratory under Cooperative Agreement Number W911NF-12-2-0022. The views and conclusions contained in this document are those of the authors and should not be interpreted as representing the official policies, either expressed or implied, of the Army Research Laboratory or the U.S. Government. The U.S. Government is authorized to reproduce and distribute reprints for Government purposes notwithstanding any copyright notation herein. The authors also acknowledge the use of the Opuntia Cluster and the advanced support from the Research Computing Data Core at the University of Houston to carry out the research presented here.

REFERENCES

- Asim, U.B., Siddiq, M.A., and Kartal, M.E., A CPFEM Based Study to Understand the Void Growth in High Strength Dual-Phase Titanium Alloy (Ti-10V-2Fe-3Al), *Int. J. Plast.*, vol. **122**, pp. 188–211, 2019.
- Azghandi, S.M., Weiss, M., Arhatari, B., Adrien, J., Maire, E., and Barnett, M., A Rationale for the Influence of Grain Size on Failure of Magnesium Alloy AZ31: An *in Situ* X-Ray Microtomography Study, *Acta Mater.*, vol. **200**, pp. 619–631, 2020.
- Benzerga, A.A., Micromechanics of Coalescence in Ductile Fracture, J. Mech. Phys. Solids, vol. 50, pp. 1331–1362, 2002.
- Benzerga, A.A. and Besson, J., Plastic Potentials for Anisotropic Porous Solids, Eur. J. Mech. A, vol. 20A, pp. 397-434, 2001.
- Benzerga, A.A. and Leblond, J.B., Effective Yield Criterion Accounting for Microvoid Coalescence, *J. Appl. Mech.*, vol. **81**, no. 3, Article ID 031009, 2014.
- Benzerga, A.A., Leblond, J.B., Needleman, A., and Tvergaard, V., Ductile Failure Modeling, *Int. J. Frac.*, vol. **201**, pp. 29–80, 2016
- Danas, K. and Ponte Castañeda, P., A Finite-Strain Model for Anisotropic Viscoplastic Porous Media: I—Theory, *Eur. J. Mech. A*, vol. **28**, pp. 387–401, 2009.
- Gologanu, M., Leblond, J.B., and Devaux, J., Approximate Models for Ductile Metals Containing Non-Spherical Voids—Case of Axisymmetric Prolate Ellipsoidal Cavities, *J. Mech. Phys. Solids*, vol. **41**, no. 11, pp. 1723–1754, 1993.
- Gologanu, M., Leblond, J.B., Perrin, G., and Devaux, J., Recent Extensions of Gurson's Model for Porous Ductile Metals, in P. Suquet, Ed., *Continuum Micromechanics, CISM Lectures Series*, pp. 61–130, New York: Springer, 1997.
- Han, X., Besson, J., Forest, S., Tanguy, B., and Bugat, S., A Yield Function for Single Crystals Containing Voids, *Int. J. Solids Struct.*, vol. **50**, pp. 2115–2131, 2013.
- Indurkar, P.P., Joshi, S.P., and Benzerga, A.A., On the Micromechanics of Void Mediated Failure in HCP Crystals, *J. Mech. Phys. Solids*, vol. **165**, Article ID 104923, 2022.
- Keralavarma, S.M. and Benzerga, A.A., An Approximate Yield Criterion for Anisotropic Porous Media, C. R. Mecanique, vol. 336, pp. 685–692, 2008.
- Keralavarma, S.M. and Benzerga, A.A., A Constitutive Model for Plastically Anisotropic Solids with Non-Spherical Voids, *J. Mech. Phys. Solids*, vol. **58**, pp. 874–901, 2010.
- Keralavarma, S.M. and Chockalingam, S., A Criterion for Void Coalescence in Anisotropic Ductile Materials, *Int. J. Plast.*, vol. **82**, pp. 159–176, 2016.
- Keralavarma, S.M., Hoelscher, S., and Benzerga, A.A., Void Growth and Coalescence in Anisotropic Plastic Solids, *Int. J. Solids Struct.*, vol. 48, pp. 1696–1710, 2011.
- Kondori, B. and Benzerga, A.A., Effect of Stress Triaxiality on the Flow and Fracture of Mg Alloy AZ31, *Metall. Mater. Trans. A*, vol. **45**, pp. 3292–3307, 2014.
- Kondori, B. and Benzerga, A.A., Modeling Damage Accumulation to Fracture in a Magnesium-Rare Earth Alloy, *Acta Mater.*, vol. **124**, pp. 225–236, 2017.
- Koplik, J. and Needleman, A., Void Growth and Coalescence in Porous Plastic Solids, Int. J. Solids Struct., vol. 24, pp. 835–853, 1988.
- Lassance, D., Scheyvaerts, F., and Pardoen, T., Growth and Coalescence of Penny-Shaped Voids in Metallic Alloys, *Eng. Frac. Mech.*, vol. **73**, pp. 1009–1034, 2006.
- Madou, K. and Leblond, J.B., A Gurson-Type Criterion for Porous Ductile Solids Containing Arbitrary Ellipsoidal Voids—I: Limit-Analysis of Some Representative Cell, *J. Mech. Phys. Solids*, vol. **60**, pp. 1020–1036, 2012a.

- Madou, K. and Leblond, J.B., A Gurson-Type Criterion for Porous Ductile Solids Containing Arbitrary Ellipsoidal Voids—II: Determination of Yield Criterion Parameters, *J. Mech. Phys. Solids*, vol. **60**, pp. 1037–1058, 2012b.
- Mbiakop, A., Constantinescu, A., and Danas, K., An Analytical Model for Porous Single Crystals with Ellipsoidal Voids, *J. Mech. Phys. Solids*, vol. **84**, pp. 436–467, 2015.
- Monchiet, V., Cazacu, O., Charkaluk, E., and Kondo, D., Macroscopic Yield Criteria for Plastic Anisotropic Materials Containing Spheroidal Voids, *Int. J. Plast.*, vol. **24**, pp. 1158–1189, 2008.
- Morin, L., Leblond, J.B., and Kondo, D., A Gurson-Type Criterion for Plastically Anisotropic Solids Containing Arbitrary Ellipsoidal Voids, *Int. J. Solids Struct.*, vol. 77, pp. 86–101, 2015.
- Noell, P.J., Sills, R.B., Benzerga, A.A., and Boyce, B.L., Void Nucleation during Ductile Rupture, *Prog. Mater. Sci.*, submitted, 2022.
- Paux, J., Morin, L., Brenner, R., and Kondo, D., An Approximate Yield Criterion for Porous Single Crystals, *Eur. J. Mech. A*, vol. **51**, pp. 1–10, 2015.
- Pineau, A., Benzerga, A.A., and Pardoen, T., Failure of Metals I. Brittle and Ductile Fracture, *Acta Mater.*, vol. 107, pp. 424–483, 2016.
- Ponte Castañeda, P. and Zaidman, M., Constitutive Models for Porous Materials with Evolving Microstructure, *J. Mech. Phys. Solids*, vol. **42**, pp. 1459–1495, 1994.
- Potirniche, G., Hearndon, J., Horstemeyer, M., and Ling, X., Lattice Orientation Effects on Void Growth and Coalescence in FCC Single Crystals, *Int. J. Plast.*, vol. **22**, pp. 921–942, 2006.
- Prasad, N.S., Narasimhan, R., and Suwas, S., Numerical Simulations of Cylindrical Void Growth in Mg Single Crystals, *Int. J. Frac.*, vol. **200**, pp. 159–183, 2016.
- Rodriguez, A.K., Ayoub, G., Mansoor, B., and Benzerga, A.A., Effect of Strain Rate and Temperature on Fracture of AZ31B Magnesium Alloy, *Acta Mater.*, vol. **112**, pp. 194–208, 2016.
- Selvarajou, B., Joshi, S.P., and Benzerga, A.A., Three Dimensional Simulations of Texture and Triaxiality Effects on the Plasticity of Magnesium Alloys, *Acta Mater.*, vol. **127**, pp. 54–72, 2017.
- Selvarajou, B., Joshi, S.P., and Benzerga, A.A., Void Growth and Coalescence in Hexagonal Close Packed Crystals, *J. Mech. Phys. Solids*, vol. **125**, pp. 198–224, 2019.
- Selvarajou, B., Kondori, B., Benzerga, A.A., and Joshi, S.P., On Plastic Flow in Notched Hexagonal Close Packed Single Crystals, J. Mech. Phys. Solids, vol. 94, pp. 273–297, 2016.
- Song, D. and Ponte Castañeda, P., A Finite-Strain Homogenization Model for Viscoplastic Porous Single Crystals: I—Theory, *J. Mech. Phys. Solids*, vol. **107**, pp. 560–579, 2017.
- Srivastava, A. and Needleman, A., Void Growth versus Void Collapse in a Creeping Single Crystal, *J. Mech. Phys. Solids*, vol. **61**, pp. 1169–1184, 2013.
- Stewart, J.B. and Cazacu, O., Analytical Yield Criterion for an Anisotropic Material Containing Spherical Voids and Exhibiting Tension-Compression Asymmetry, *Int. J. Solids Struct.*, vol. 48, pp. 357–373, 2011.
- Torki, M.E., Benzerga, A.A., and Leblond, J.B., On Void Coalescence under Combined Tension and Shear, *J. Appl. Mech.*, vol. **82**, no. 7, Article ID 071005, 2015.
- Tvergaard, V., On Localization in Ductile Materials Containing Spherical Voids, Int. J. Frac., vol. 18, pp. 237–252, 1982.
- Yang, Q. and Ghosh, S., A Crystal Plasticity Model for Porous HCP Crystals in Titanium Alloys under Multiaxial Loading Conditions, Int. J. Solids Struct., vol. 238, Article ID 111400, 2022.
- Yerra, S.K., Tekoglu, C., Scheyvaerts, F., Delannay, L., Van Houtte, P., and Pardoen, T., Void Growth and Coalescence in Single Crystals, *Int. J. Solids Struct.*, vol. 47, pp. 1016–1029, 2010.
- Zhang, J. and Joshi, S.P., Phenomenological Crystal Plasticity Modeling and Detailed Micromechanical Investigations of Pure Magnesium, *J. Mech. Phys. Solids*, vol. **60**, pp. 945–972, 2012.